PCCP

Accepted Manuscript

ROYAL SOCIETY OF CHEMISTRY

www.rsc.org/pccp

Spin effects in thermoelectric phenomena in SiC nanoribbons

K. Zberecki[1], **R. Swirkowicz**[1], **M. Wierzbicki**[1], **J. Barnaś**[2]

Using *ab-initio* methods we calculate thermoelectric and spin thermoelectric properties of zigzag SiC nanoribbons, asymmetrically terminated with hydrogen. Such nanoribbons display ferromagnetic ground state, with edge magnetic moments oriented in parallel. Both thermopower and spin thermopower have been determined as a function of chemical potential and temperature. To find the thermoelectric efficiency, the total heat conductance has been calculated, i.e. the electronic and phonon contributions. Numerical results for SiC nanoribbons are compared with those for graphene and silicene ones.

1 Introduction

One can observe recently a growing interest in thermoelectric properties of various nanostructures. This is because thermoelectric phenomena in such systems offer a possibility to convert dissipated heat into electric energy at a nanoscale. Recent investigations show that the thermopower and thermoelectric efficiency in nanostructures can be considerably enhanced due to quantum size effect and Coulomb blockade [1–4]. Moreover, the interplay of charge, spin and heat transport in magnetic nanostructures can lead to spin related thermoelectric phenomena [5–8]. In particular, when the spin relaxation time in such systems is sufficiently long, then – apart from the conventional thermopower S_c corresponding to the thermal generation of a charge voltage ΔV – the spin thermopower S_s can be observed, which describes the spin voltage ΔV_s induced by a temperature gradient ΔT [8]. The spin thermoelectric phenomena can play an important role in spintronic devices, where dissipated heat can be converted into a spin voltage [7].

Very recently both conventional and spin thermoelectric effects in zigzag-type nanoribbons of graphene (zGNRs) and silicene (zSiNRs) have been investigated theoretically [9–16]. Such nanoribbons exhibit antiferromagnetic ground state, where magnetic moments are localized mainly at the edge atoms and the moments at one edge are opposite to those at the other edge [17,18]. Ferromagnetic alignment of the edge moments in zGNRs and zSiNRs can be achieved due to the proximity effect (exchange coupling of the moments to a ferromagnetic substrate), external magnetic field [16–20], or appropriate modifications of the edges [21–24]. As the spin thermoelectric effects disappear in a strictly antiferromagnetic state, they become observable in the ferromagnetic phase. Indeed, it has been shown that a considerable spin S_s and conventional S_c thermopowers can be observed in ferromagnetic nanoribbons [15]. The effect can be further enhanced by structural defects like antidots [14], impurity atoms [25], or asymmetric hydrogenation of the edge atoms [26]. As a result, the thermoelectric efficiency of such systems can be enhanced in comparison to that in other materials, which makes these structures attractive for applications.

Apart from graphene and silicene, also other two-dimensional structures based on a honey-comb lattice have been investigated – mostly theoretically by *ab-initio* methods. One of such graphene-like materials is two-dimensional silicon carbide (SiC), which in contrast to graphene or silicene is a wide-band semiconductor [27,28]. Therefore, this material is very promising for future applications in nanoelectronics devices, and has received a considerable attention recently. Though two-dimensional SiC has not been obtained yet, various low-dimensional SiC structures, like one-dimensional SiC nanotubes and nanowires have been synthesized [29,30]. Apart from this, various techniques for growing SiC nanostructures have been proposed [31–35].

Using first-principles methods, the structural and electronic properties of SiC nanoribbons (SiCNRs) have been investigated theoretically [36–44]. It has been shown, among others, that magnetization of zigzag SiC nanoribbons (zSiCNRs) can be controlled by an external transverse electric field [39]. Furthermore, a half-metallic behavior has been found in narrow zigzag SiCNRs [36]. Studies of zSiCNRs doped with B and N atoms show that the half-metallic behavior is maintained in the presence of boron impurities, whereas nitrogen atoms at the edge positions transform the nanoribbon into the metallic phase [45]. Interestingly, it has been also shown that magnetic properties of zSiCNRs can be controlled by appropriate modification of the edges, e.g. with donor/acceptor groups [44] or F/Cl atoms [43].

[1] *Faculty of Physics, Warsaw University of Technology,ul. Koszykowa 75, 00-662 Warsaw, Poland*
[2] *Faculty of Physics, Adam Mickiewicz University, ul.Umultowska 85, 61-614 Poznań, Poland*
and Institute of Molecular Physics,Polish Academy of Sciences, Smoluchowskiego 17, 60-179 Poznań, Poland

Stability of zSiCNRs with bare edges as well as with edges terminated with hydrogen has been studied and discussed in several papers [38,46], and a reconstruction of the bare edges, especially of C type, has been proposed. However, termination with hydrogen can prevent the reconstruction, and thus enhance the binding energy [38,46,47]. Theoretical studies show that different types of hydrogen terminated zSiCNRs can be obtained by controlling hydrogen pressure in the environment. For low hydrogen pressure, structures of the 1H-1H type can be formed, where atoms at both edges are terminated with single H atoms. However, under standard conditions the most stable nanoribbons are those of 2H-2H type, with both Si and C edge atoms bonded to two hydrogen atoms, or nanoribbons asymmetrically terminated with hydrogen, i.e. of the 2H-1H type, where the C edge atoms are bonded to single hydrogen atoms only [46]. Calculations for zSiCNRs of 1H-1H type show, that the ferromagnetic configuration, where all edge magnetic moments are ordered in parallel, is practically degenerate with the antiferromagnetic state, in which magnetic moments at one edge are antiparallel to those at the other edge [46]. The latter configuration is very interesting due to half-metallic behavior, but in practice it would be difficult to stabilize the antiferromagnetic ordering. On the other hand, nanoribbons of 2H-2H as well as of 2H-1H types exhibit ferromagnetic ground state.

In the present paper we focus on the nanoribbons asymmetrically terminated with hydrogen, i.e. on the nanoribbons of 2H-1H type, which exhibit a stable ferromagnetic ordering at relatively low temperatures. At higher temperatures, the ferromagnetic state can be stabilized by an external magnetic field or by the proximity effect. For these systems we calculate transport and spin related thermoelectric coefficients, and show that a considerable enhancement of the thermoelectric efficiency can be expected even at room temperature. In section 2 we introduce the thermoelectric coefficients and present numerical results on the electrical and heat conductance as well as on the thermopowers. The phonon heat conductance is presented and discussed in section 3. Thermoelectric efficiency of zSiCNRs is calculated and described in section 4. Comparison with other related systems is given in section 5, while summary and final conclusions are in section 6.

2 Thermoelectric properties of 2H-1H zSiC-NRs

2.1 Method of calculations

Electronic properties of zSiCNRs were investigated by the *ab-initio* method within the DFT Siesta code [53]. The structure under consideration was optimized until atomic forces converged to 0.02 eV/A. The atomic double polarized basis (DZP) was used, and the grid mesh cutoff was set equal to 200 Ry. The generalized gradient approximation (GGA) with Perdew-

Burke-Ernzerhof (PBE) parametrization was applied for the exchange-correlation part of the total energy functional [55]. Calculations based on the Lee-Yang-Parr (LYP) parametrization of the GGA potential [56] were also performed, and the results of both methods were compared. Then, the spin-resolved transmission $T_\sigma(E)$ through the nanoribbon was determined within the non-equilibrium Green function (NEGF) method, as implemented in the Transsiesta code [54].

In a ferromagnetic nanoribbon, in which the two spin channels are different and not mixed on the length scale comparable to the nanoribbon length, spin effects become important and have a significant impact on transport and thermoelectric properties. Apart from the voltage ΔV, also a spin voltage ΔV_s can be then generated by a temperature gradient ΔT [26]. Therefore, the conventional (charge) S_c as well as spin S_s thermopowers can be introduced as $S_c = -\Delta V/\Delta T$ and $S_s = -\Delta V_s/\Delta T$, respectively. Both S_c and S_s can be determined under the conditions that the charge I and spin I_s currents are equal to zero. Then, in the linear response regime, the conventional and spin thermopowers can be calculated from the formulas [26]

$$S_c = -\frac{1}{2|e|T}(L_{1\uparrow}/L_{0\uparrow} + L_{1\downarrow}/L_{0\downarrow}),$$
$$S_s = -\frac{1}{2|e|T}(L_{1\uparrow}/L_{0\uparrow} - L_{1\downarrow}/L_{0\downarrow}), \qquad (1)$$

where $L_{n\sigma} = -\frac{1}{h}\int dE\, T_\sigma(E)(E-\mu)^n \frac{\partial f}{\partial E}$ with n=0,1,2. Here, $T_\sigma(E)$ is the spin-dependent transmission function, $f(E-\mu)$ is the Fermi-Dirac distribution function corresponding to the chemical potential μ and temperature T (equal in both electrodes in the linear response description). It should be mentioned that S_c and S_s can be also determined in another way, namely S_c can be defined for $I = 0$ and $\Delta V_s = 0$, while S_s for $I_s = 0$ and $\Delta V = 0$ [26]. The two different definitions of S_c and S_s depend essentially on experimental conditions. In the former definition the thermally-induced voltages ΔV and ΔV_s are determined for zero charge and spin currents, while in the latter case some spin (charge) current can generally flow when measuring ΔV (ΔV_s). In the following we will use the definitions (1) for S_c and S_s.

The electrical conductance of the spin-σ channel is determined by the kinetic coefficient $L_{0\sigma}$ as $G_\sigma = e^2 L_{0\sigma}$, while the electronic contribution κ_e to the thermal conductance is given by

$$\kappa_e = \frac{1}{T}\sum_\sigma \left(L_{2\sigma} - \frac{L_{1\sigma}^2}{L_{0\sigma}}\right). \qquad (2)$$

Accordingly, the conventional and spin thermoelectric efficiency can be defined as [26]

$$ZT_c = \frac{S_c^2(G_\uparrow + G_\downarrow)T}{\kappa}, \quad ZT_s = \frac{S_s^2|G_\uparrow - G_\downarrow|T}{\kappa}, \qquad (3)$$

where $\kappa = \kappa_e + \kappa_{ph}$ is to the total thermal conductance, which includes both electronic κ_e and phonon κ_{ph} contributions.

2.2   Results

As already mentioned above, at ambient conditions the zSiC-NRs of 2H-1H type can be stable. Calculations performed for nanoribbons containing $N = 6$ zigzag chains show that such nanoribbons are ferromagnetic in the ground state, with magnetic moments localized mainly on the C edge atoms and on the C atoms adjacent to the Si edge sites. It is interesting that the Si edge atoms do not posses magnetic moments, see Fig. 1.
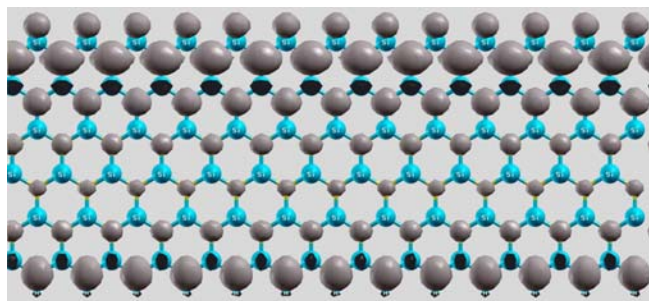

Fig. 1 (Color online) Spin density distribution in the ferromagnetic ground state, calculated for the zSiCNR of 2H-1H type. One H atom is attached to each C edge atom while two H atoms are attached to each Si edge atom. Black and grey dots represent magnetic moments of opposite orientations.

Energy of the nanoribbon part presented in Fig. 1 in the ferromagnetic state is lower by 0.009 eV than the energy in the corresponding ferrimagnetic state (in which the edge moments are antiparallel but not fully compensated). In turn, energy of the corresponding nonmagnetic state is much higher. As the ferromagnetic configuration can be easily stabilized by an external magnetic field or by the proximity effect, in the following we consider only this configuration as the most stable one. The spin-dependent band structure and the transmission function $T_\sigma(E)$, calculated within GGA with the use of the PBE potential are presented in Fig. 2. Similar results were also obtained using the LYP potential. Results obtained by other authors are consistent with those in Fig. 2 [47], which indicates that they are reliable and can be considered as a good base for discussion of the transport properties of zSiCNRs. As follows from Fig. 2, the system is a ferromagnetic semiconductor with a narrow gap, smaller than 0.1 eV, which opens in the vicinity of the Fermi energy E_F in the spin-down channel, whereas a very wide gap appears in the spin-up channel. Accordingly, transport properties of the system for chemical potentials near E_F (corresponding to μ=0) is fully determined by the carriers in the spin-down channel, especially by electrons from the flat band lying just above the Fermi level. This band leads
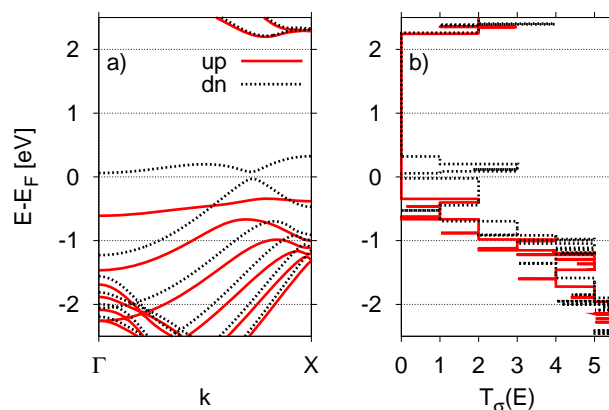

Fig. 2 (Color online) Spin-resolved band structure (a) and the transmission function (b), calculated for a zSiCNR of 2H-1H type with N=6 zigzag chains.

to high transmission function $T_\downarrow$ for energies slightly above E_F. Below the Fermi energy, $T_\downarrow$ is flat in a relatively wide energy region. On the other hand, the spin-up channel is nonconductive in a wide energy region below and above E_F, as $T_\uparrow$ is there roughly equal to zero. Such a behavior has a strong influence on electric and thermoelectric properties of the ribbon. As presented in Fig. 3, in a wide range of the chemical potential μ below and above the Fermi energy, the electrical conductance is dominated by the spin-down carriers and exhibits almost 100% spin polarization.
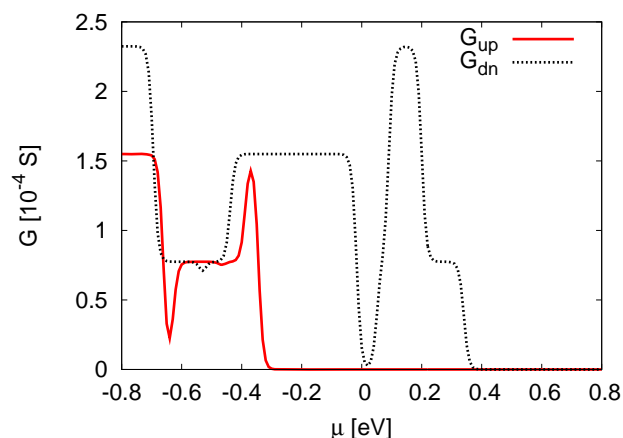

Fig. 3 (Color online) Spin-resolved electrical conductance G_σ (G_{up} for the spin-up and G_{dn} for the spin-down channels) calculated for the zSiCNR with $N = 6$ zigzag chains and for $T = 90$K.
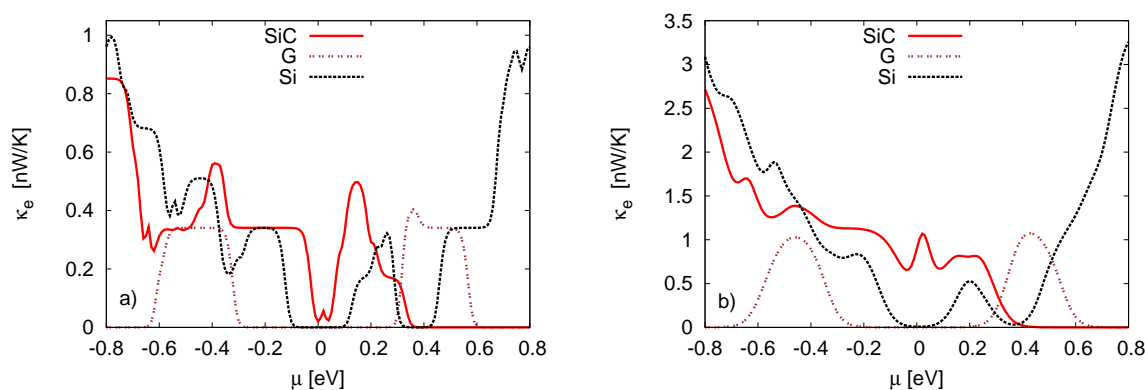
Fig. 4 (Color online) Electronic contribution, κ_e, to the thermal conductance of the 2H-1H zSiCNR, calculated for $N = 6$ and for $T = 90$K (a) and $T = 300$K (b). Similar data for graphene (G) and silicene (Si) nanoribbons are also shown for comparison.

The spin-up channel contributes to the conductance for negative μ, below -0.3 eV. This region, however, is less important, as it is difficult to be achieved. Therefore, the system can work as a very efficient spin filter in the semiconducting transport regime, contrary to the well-known half-metallic spin filters. Thus, the system may be interesting for applications in specific spintronic devices. The narrow energy gap near E_F can be well visible at low temperatures in both the electrical conductance G (Fig. 3) and in the electronic contribution κ_e to the thermal conductance (Fig. 4a).

One should also note that both electrical and thermal conductances are practically constant in a wide range of negative μ, which corresponds to flat transmission in the conductive spin-down channel and blocked spin-up channel. The thermal conductance κ_e considerably increases for large negative μ, where the spin-up channel becomes active and contributes to the conductance. The thermal conductance also strongly increases with temperature, compare Fig. 4a) and Fig. 4b). It is interesting to note, that despite the energy gap in the vicinity of the Fermi energy, κ_e is enhanced and exhibits there a local maximum, which can be related to a rapid increase in transmission near the edges of the gap in the spin-down channel and to a thermal smearing of the Fermi-Dirac distribution function. Note, the peak in thermal conductance appears despite of the lack of such a peak in the electrical conductance. This is due to the fact, that the contributions to electrical current from electrons and holes almost compensate at this point, while the electron and hole contributions to the heat current add then constructively. For higher values of μ, the thermal conductance is practically constant and much lower as the transmission in the spin-down channel is reduced. Furthermore, κ_e smoothly decreases, when the very wide energy gap is approached.

The very steep changes in transmission near the low-energy edge of the gap in the spin-up channel ($\mu < 0$) generate a high thermopower, whose maximum appears at a distance of several kT from the gap edge, see Fig. 5a) and Fig. 5c). Since the main contribution originates from the spin-up holes, both conventional S_c and spin S_s thermopowers are positive and both are practically equal. The transmission $T_\downarrow$ is flat near the edge of spin-up gap, so there is no contribution from the spin-down channel. A strong enhancement of the thermopower can be also observed for $\mu > 0$, in the vicinity of μ=0.4 eV. Now, S_c and S_s have opposite signs, which indicates that the thermopower is due to rapid changes in the transmission $T_\downarrow$ near the edge of the energy gap. The spin-up channel is then nonconductive with $T_\uparrow = 0$, so it does not contribute to the thermopower. Additional structure can be also observed in a close vicinity of E_F, which corresponds to changes in the spin-down transmission due to the narrow energy gap in this channel. However, since the gap is very narrow, the peaks are much lower as positive and negative contributions due to holes and electrons partially compensate each other. High values of the thermopower can be observed only when both contributions are well separated and this requires relatively wide gaps or low temperatures.

Figures 5b) and 5d) present the conventional and spin thermopowers, calculated for the room temperature. Due to a considerable broadening of the Fermi-Dirac distribution function, the peaks in thermopowers S_c and S_s are strongly broadened and the main peak is shifted towards higher values of the chemical potential. Since the energy gap in the spin-up channel is very wide and exceeds 2.5 eV, there is no contribution to S_c and S_s from electrons in the conduction band, even at high temperatures.*

---

* To avoid artificial enhancement of the thermopower for μ in the wide energy gap, we set $S = 0$ in those regions where the denominator in formulae (1) was
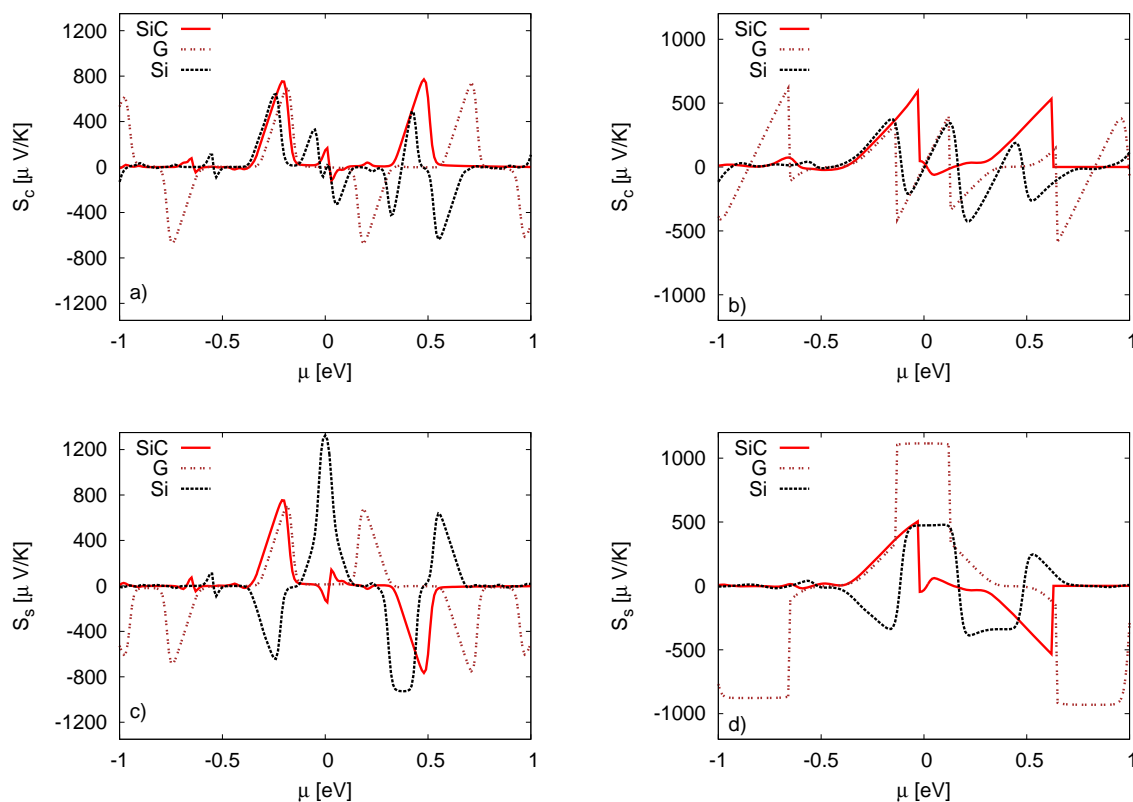
Fig. 5 (Color online) Charge, S_c, and spin, S_s, thermopowers calculated for the $N = 6$ zSiCNR of 2H-1H type at $T = 90$K (a,c) and $T = 300$K (b,d). The corresponding data for graphene (G) and silicene (Si) nanoribbons are also shown for comparison.

3 Phonon heat conductance

Numerical calculations of the phonon contribution to the heat conductance were performed with the fast semiempirical molecular orbital package MOPAC [48,49]. The geometries of nanoribbons were optimized with the PM7 semiempirical Hamiltonian [50] in the restricted Hartree-Fock (RHF) approximation using the eigenfollowing (EF) procedure. The geometry convergence criteria for the gradient norm was 0.1 kcal/mol/Å. The heat of formation of the obtained structures was stationary. The mass-weighted hessian matrix of second derivatives of energy with respect to atomic displacements from stationary positions was determined by the MOPAC FORCE calculations.

The phonon band structure was determined by the cluster method [51] (also called direct method). The large unit cell (LUC) consisting of 7 elementary unit cells of a zigzag nanoribbon was utilized. The LUC must be large enough, because the atomic orbitals of the center unit cell (CUC) should

smaller than the error of integration method used to calculate $L_{n\sigma}$.

not significantly overlap with those at the end of the cluster. A single Γ-point FORCE calculation utilizing Born-von Karman condition for the LUC is sufficient to determine the phonon band structure. The phonon frequencies were obtained from the eigenvalues of the Fourier transform of the submatrices of mass-weighted hessian matrix, describing the elastic interaction of CUC with other cells in the cluster.

An example of the phonon-band structure for the $N = 7$ zSiCNR is presented in Fig. 6, together with the respective phonon transmission function T_{ph}. Two high-frequency bands around $\nu = 2000$ cm^{-1}, which result mainly from vibrations of the hydrogen atoms, are not presented in Fig. 6, as they do not influence the phonon thermal conductance.

In the linear-response approximation, the phonon conductance κ_{ph} can be obtained from the phonon transmission T_{ph} by the following formula

$$\kappa_{ph} = h \int_0^\infty \omega\, T_{ph}(\omega) \frac{\partial f_B(\omega)}{\partial T}\, d\omega, \qquad (4)$$

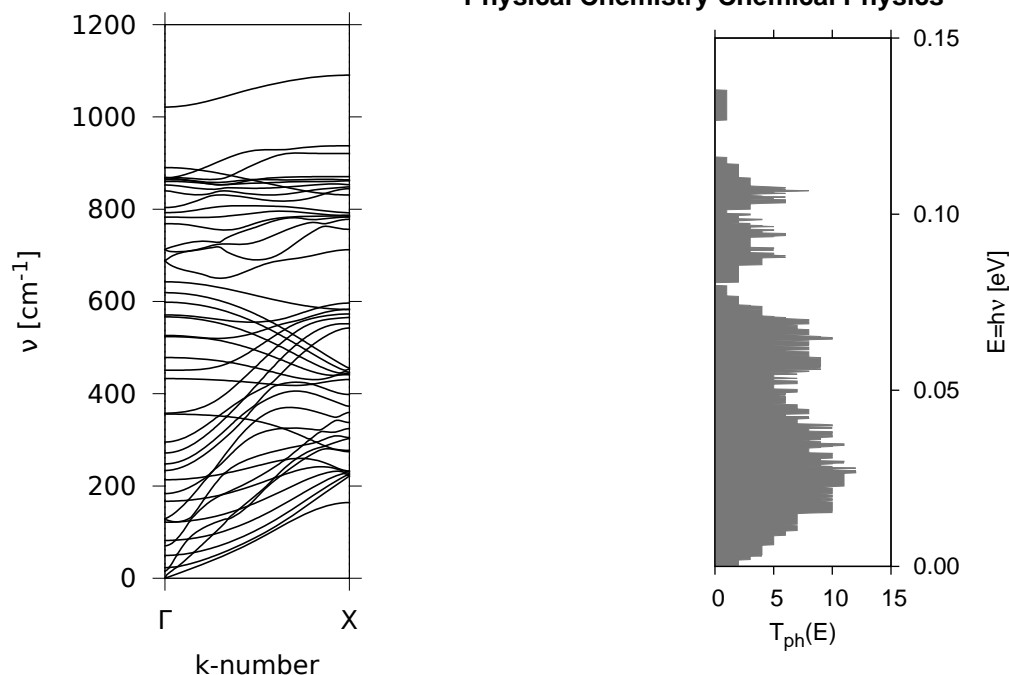where f_B is the Bose-Einstein distribution for thermal phonons

Fig. 6 Phonon band structure and phonon transmission function for the SiC zigzag nanorribon with $N = 7$.

at temperature T. Equation (4) may be expressed as integral over phonon energy $\varepsilon = \hbar\omega$ in electronvolts, multiplied by the combination of physical constants $ek/h = 3.3384 \cdot 10^{-9}$. The phonon conductance expressed in nanowatts per Kelvin can be then calculated from the formula

$$\kappa_{ph} \,[\text{nW/K}] = 3.3384 \cdot \frac{1}{(kT)^2} \int\limits_0^\infty \varepsilon^2 T_{ph}(\varepsilon) \frac{e^{\varepsilon/kT}}{(e^{\varepsilon/kT} - 1)^2} \, d\varepsilon. \tag{5}$$

Figure 7 presents the phonon thermal conductance as a function of the nanoribbon width of zSiCNRs, determined from the formula (5). This figure shows that the dependence on the nanoribbon width is approximately linear, and that the heat conductance increases with temperature.

3.1 Comparison with the force constants model

In order to test validity of the results obtained from the MOPAC calculations for a new material such as silicon carbide nanoribbons, we compared the phonon thermal conductance for zigzag graphene nanoribbons (ZGNRs) determined by MOPAC with the results from the well-established fourth nearest neigbours force constants model (4NNFC)[52].

In the MOPAC calculations, the geometries of zGNRs were optimized with the same convergence criteria as for SiC nanoribbons. All zGNRs were hydrogenated, with two hydrogen atoms per unit cell. The 4NNFC is a topological
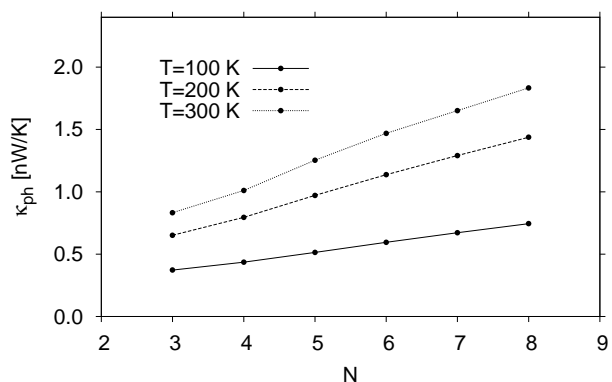

Fig. 7 Phonon thermal conductance of the SiC zigzag nanoribbons as a function of the number of zigzag chains, N. Different curves correspond to indicated temperatures.

model. The force constants depend only on the order of neighbors, and not on the exact position of the atoms, which are assumed to be already in the equilibrium positions. Therefore, the geometry optimization is unnecessary. Interactions up to the fourth neighbors require two-adjacent unitary cells in the construction of the dynamical matrix. Diagonalization of the resulting dynamical matrix yields frequencies of the vibrations, which depend on the one-dimensional wave-vector, $0 < k < \pi/a$, where a is the length of the nanoribbon's unit
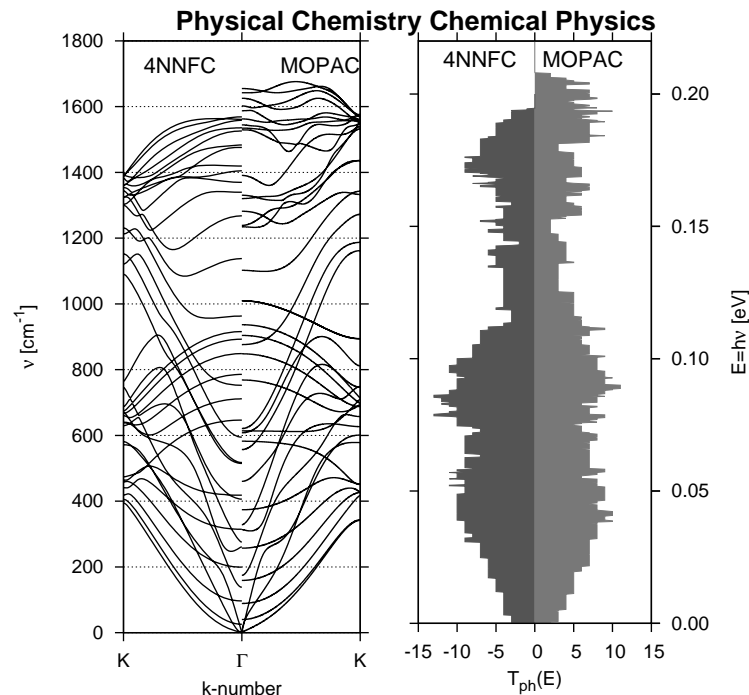
Fig. 8 Phonon band structure (left) and transmission function (right) for the $N = 6$ zGNR, determined by the MOPAC program and from the 4NNFC model.
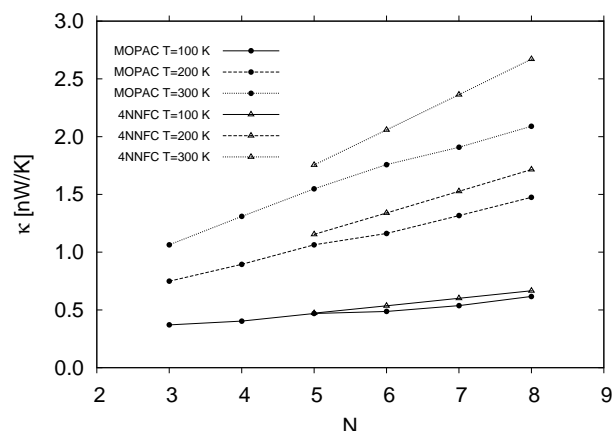
cell.

Fig. 9 Phonon thermal conductance κ_{ph} of zigzag graphene nanoribbons as a function of of number N of zigzag chains, determined by the MOPAC program and from the 4NNFC model for indicated temperatures.

Figure 8 presents the phonon band structure and the corresponding transmission function of the $N = 6$ zGNR, calculated by the MOPAC program and from the 4NNFC model. The general structure of the bands is similar, except an overall difference in energy scale factors. All the bands predicted by the 4NNFC model are below 1600 cm^{-1}. This may be explained by the fact that the 4NNFC model does not take into account the hydrogen bonds at the nanoribbons' edges.

Figure 9 presents the phonon thermal conductance κ_{ph} as a function of zGNR's width and temperature. For low temperature, $T = 100$ K, the results obtained by both methods are in excellent agreement. For higher temperature, $T = 200$ K, the difference for wider zGNRs is about 15 %, while for higher temperature, $T = 300$ K, the difference for $N = 8$ zGNR is about 20 %. The semiempirical PM7 method contained in the MOPAC program is based on the Hartree-Fock approximation to the quantum many-electron problem. In contrast, the 4NNFC model is based on a simple classical-mechanics description of the chemical bonds as coupled harmonic oscillators. In view of the fundamental difference between both methods, the maximum difference of 20 % seems acceptable. We consider the thermal conductance of zGNRs obtained from the MOPAC, and therefore also that of zSiCNRs, as reliable.

4 Thermoelectric efficiency of zSiCNRs of 2H-1H type

The conventional ZT_c and spin ZT_s thermoelectric efficiency of zSiCNRs have been calculated according to the formulae (3). The phonon contribution to the total thermal conductance

plays an important role and affects the final values of ZT_c and ZT_s. The phonon contribution for free-standing nanoribbons was calculated in the previous section within the MOPAC approach. On the basis of the analysis presented there, one may conclude that the calculated κ_{ph} can be somewhat underestimated, especially at high temperatures. On the other side, the phonon conductance can be modified by the presence of substrate, defects, and the edge roughness, which were not taken into account in our calculations. Therefore, we estimate the efficiency by assuming κ_{ph} can vary from $\kappa_1 = \kappa_{ph}^{\text{MOPAC}}$ to $\kappa_2 = 2\kappa_{ph}^{\text{MOPAC}}$ (so we admit that the calculated value of the phonon conductance using MOPAC procedure can be underestimated up to a factor of 2). The results obtained for ZT_c and ZT_s as a function of the chemical potential are presented in Fig. 10 for two different temperatures, $T = 90K$ and $T = 300K$.

For each temperature two curves are presented, one (the solid line) corresponding to the phonon contribution κ_1 and the second one (the dashed line) corresponding to κ_2. Accordingly, the efficiency can take values from the regions limited by solid and dashed lines. It is interesting that in any case both conventional and spin thermoelectric efficiencies are strongly enhanced, even though the contribution to κ_{ph} can be overestimated when κ_2 is used, especially at low temperatures.

The presented results clearly show that the phonon conductance rather strongly influences the thermoelectric efficiency, but the effect is not so crucial as in graphene nanoribbons. It is mainly due to a fact that the electron thermal conductance in zSiCNRs is relatively high – it is higher than in similar asymmetric zGNRs and zSiNRs (Fig. 4). At low temperatures ($T = 90K$) both ZT_c and ZT_s exhibit a very well pronounced peak in the vicinity of μ=-0.2 eV. This peak corresponds to the maximum in S_c and S_s, and comes from the rapid decrease in the spin-up transmission. With increasing temperature, this maximum shifts towards higher energies and becomes wider. Accordingly, zSiCNRs asymmetrically terminated with hydrogen, which have a wide energy gap in one spin channel, exhibit high thermoelectric efficiency, and therefore are promising for applications in nanodevices for energy conversion at nanoscale.

5 Comparison of thermoelectric efficiency of C and Si based nanoribbons

Since the thermoelectric phenomena in graphene (zGNRs) and silicene (zSiNRs) nanoribbons have been widely studied, we find it instructive to discuss and compare the results obtained for these structures with the results for zSiCNRs. Only systems asymmetrically terminated with hydrogen atoms of the 2H-1H type are considered. Ab-initio calculations show that the ground state of these structures is semiconducting with fer-

romagnetic ordering of magnetic moments. The energy of the non-magnetic state is relatively high, higher than the thermal energy at room temperature. Therefore, we consider ferromagnetic ribbons only. In any case, this state can be stabilized by an external magnetic field. The calculated thermoelectric efficiency at low (90K) and room temperatures is depicted in Fig. 11 for all the structures under consideration.

The phonon conductance, which has a significant influence on the thermoelectric efficiency, was calculated as a function of temperature in our earlier papers for graphene [14] and silicene [15] nanoribbons within the 4NNFC approach. As discussed in sec. 3 of the present paper, in the case of zGNRs this conductance is higher than that determined with the use of MOPAC procedure, especially at room temperature (Fig. 9). Therefore, one can assume that the 4NNFC method, which is commonly used, at least for zGNRs, gives more reliable results than the MOPAC one, and we calculate thermoelectric efficiency with κ_{ph} determined using this approach. The low temperature ZT_c and ZT_s for zSiNRs of 2H-1H type were already presented in our earlier paper [26], but it seems to be instructive to compare here the results for all systems. The thermoelectric efficiency of zSiNRs decreases with increasing temperature, though the contributions to thermal conductance due to electrons, κ_e (Fig. 4b), and due to phonons [15] are relatively low. Note, that in the region of small $|\mu|$, κ_e calculated for zSiNRs is much lower than the one obtained for zSiCNRs. The reduced efficiency in zSiNRs results from the fact that the thermopower decreases with increasing temperature. According to Fig. 5, both S_c and S_s in zSiNRs achieve at room temperature lower values than at $T = 90K$, especially the main central peak in S_s is considerably reduced and broadened. Due to relatively narrow energy gaps in the spin-up and spin-down channels, both holes and electrons contribute to the thermopower, but with opposite signs, so at higher temperatures these contributions partially cancel [26]. Then, S_c oscillates with the chemical potential, taking relatively small values (Fig. 5). In turn, the spin thermopower S_s achieves slightly higher values in the vicinity of the Fermi energy, as the contributions from the spin-up holes partially overlap with the contributions from the spin-down electrons. All these changes in S_c and S_s influence ZT_c and ZT_s, and reduce the thermoelectric efficiency (Fig. 11). However, the efficiency is still relatively high at room temperature.

Very interesting results are obtained for zGNRs asymmetrically terminated with hydrogen. Our calculations show that 2H-1H zGNRs can exhibit ferromagnetic ordering, even at high temperatures. It should be noted that both ZT_c and ZT_s are remarkably enhanced at room temperature, despite of high phonon thermal conductance (Fig. 11). On the other hand, negligibly small efficiency is obtained at 90K. This behavior directly results from a peculiar band structure of the 2H-1H zGNRs, which reveals the presence of two flat bands – one
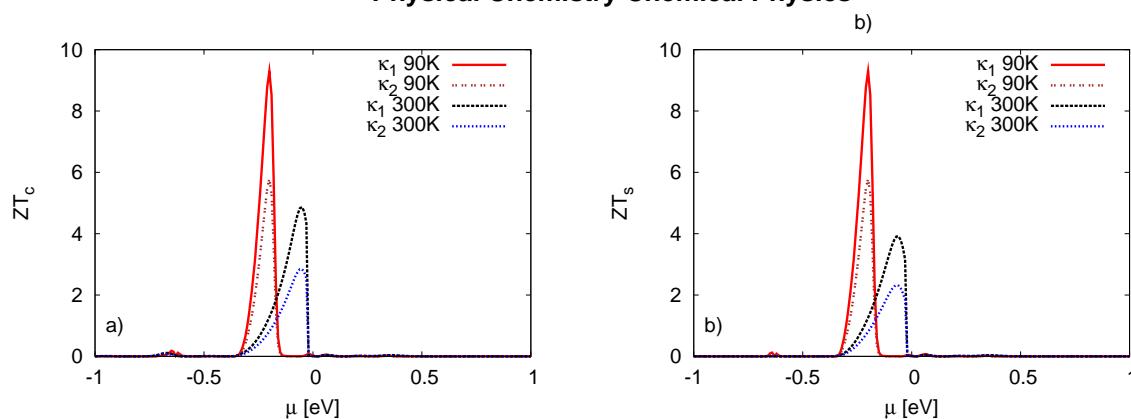
Fig. 10 (Color online) Conventional, ZT_c, and spin ZT_s, thermoelectric efficiency in the $N = 6$ zSiCNRs of 2H-1H type, calculated for $T = 90K$ and $T = 300K$ and for two different phonon conductances (see the text).
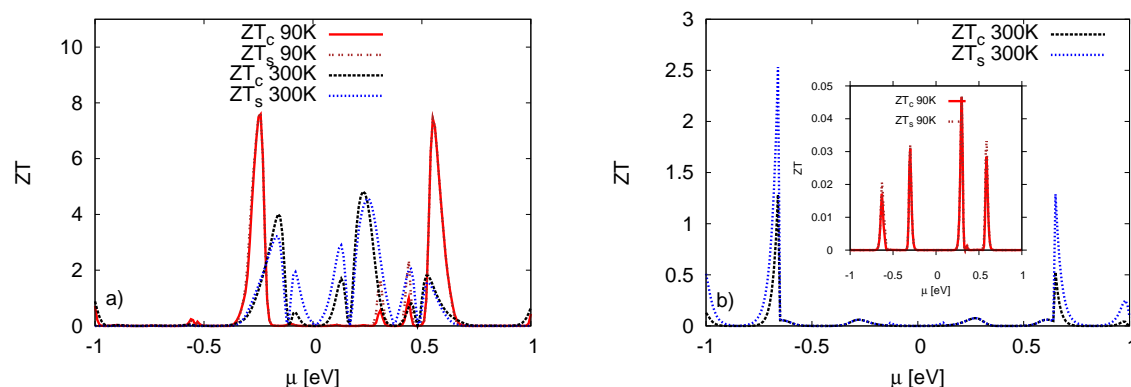

Fig. 11 (Color online) Conventional, ZT_c, and spin ZT_s, thermoelectric efficiency, calculated for $N = 6$ zSiNRs (a) and $N = 6$ zGNRs (b) of 2H-1H type for $T = 90K$ and $T = 300K$.

below (spin-up channel) and one above (spin-down channel) the Fermi level – which are separated by a relatively wide gap of the order of 0.7 eV. Moreover, wide gaps of the order of 1.5 eV occur both in the spin-up and spin-down channels. Presence of these gaps has a strong influence on the transmission function, and therefore also on the conductance and thermoelectric properties. The thermal conductance due to electrons is relatively low, even at room temperature, and a wide gap between the two flat bands is well visible in the vicinity of the Fermi level (Fig. 4a,b). The presence of wide energy gap, both in the spin-up and spin-down channels, strongly enhances the spin-up and spin-down thermopowers, as the contributions due to holes and electrons in both spin channels do not compensate each other, and finally, S_c and S_s increase considerably. Accordingly, a remarkable increase of the thermoelectric efficiency (Fig. 11) in the 2H-1H zGNRs can be observed

at room temperature, despite the phonon conductance is then quite large. However, relatively large changes in the chemical potential would be required to achieve the high efficiency.

6   Summary and conclusions

We have studied asymmetrically hydrogenated zigzag SiC nanoribbons of the 2H-1H type, with ferromagnetic ordering of the edge magnetic moments. The achieved numerical results reveal a remarkable spin thermoelectric phenomena at low and room temperatures. The considerable enhancement of the thermopower results from a peculiar band structure of the nanoribbons, with a wide energy gap in one of the spin channels, which leads to steep changes in transmission at the low-energy edge of the gap. The main contribution to the thermopower comes then from the holes in this spin channel.

Following this, also a remarkable increase of the thermoelectric efficiency can be expected. Moreover, zSiCNRs of 2H-1H type exhibit 100% spin polarization of electric current for certain regions of chemical potential. Thus, they can work as very efficient spin filters, which makes them interesting for application in spintronics devices.

The results have been compared with those obtained earlier for zSiNRs and zGNRs of 2H-1H type. In zSiNRs with ferromagnetic ordering, both thermopower and thermoelectric efficiency are strongly suppressed at room temperature. Our calculations show that in such nanoribbons, the electron and hole contributions to the thermopower partially cancel each other at higher temperatures due to relatively narrow energy gaps in both spin channels. Furthermore, our analysis shows that the thermoelectric phenomena in zGNRs asymmetrically terminated with hydrogen atoms can be enhanced at room temperature. However, the corresponding peaks appear at relatively high values of $|\mu|$, and this region may be rather difficult to be achieved.

7 Acknowledgments

References

1 R. Venkatasubramanian, E. Siivola, T. Colpitts, B. O'Quinn, Nature 413, 597 (2001).

2 A. I. Hochbaum, R. Chen, R.D. Delgado, W. Liang, E.C. Garnett, M. Najarian, A. Majumdar, P. Yang, Nature 451, 163 (2008).

3 T.C. Harman, P.J. Taylor, M.P. Walsh, B.E. LaForge, Science 297, 2229 (2002).

4 N.B. Duarte, G.D. Mahan, S. Tadigadapa, Nano Lett. 9, 617 (2009).

5 M. Walter, J. Walowski, V. Zbarsky, M. Mnzenberg, M. Schfers, D. Ebke, G. Reiss, A. Thomas, P. Peretzki, M. Seibt, J.S. Moodera, M. Czerner, M. Bachmann, Ch. Heiliger, Nature Mat. 10, 742 (2011).

6 N. Liebing, S. Serrano-Guisan, K. Rott, G. Reiss, J. Langer, B. Ocker, H.W. Schumacher, Phys. Rev. Lett. 107, 177201 (2011).

7 K. Uchida, S. Takahashi, K. Harii, J. Ieda, W. Koshibae, K. Ando, S. Maekawa, E. Saitoh, Nature 455, 778 (2008).

8 M. Wierzbicki, R. Swirkowicz, and J. Barnaś, Phys. Rev. B80, 195409 (2009)

9 F.Mazzamuto, V.Huang Nguyen, Y.Apertet, C.Caer, C.Chassat, J.Saint-Martin and P.Dollfus, Phys. Rev. B83, 235426 (2011)

10 Y. Ding and J. Ni, Appl/ Phys. Lett. 95, 083115 (2009); W.Zhao, Z.X.Guo, J.X.Cao, and J.W. Ding, AIP Advances 1, 042135 (2011).

11 T.G.Pedersen,C.Flindt,J.Pedersen,   N.A.Mortensen, A.P.Jauho, and K.Pedersen, Phys. Rev. Letters 100, 136804 (2008).

12 Y.Yan, Q.F.Liang, H.Zhao, C.Q.Wu, and B.Li, Phys. Letters A 376, 2425 (2012).

13 X.Ni,G.Liang, J.-S.Wang, and B.Li, Appl. Phys. Lett. 95,192114 (2009).

14 M.Wierzbicki, R.Swirkowicz and J.Barnaś, Phys. Rev. (2013)

15 K.Zberecki, M.Wierzbicki, J. Barnaś, R. Swirkowicz, Phys. Rev B (2013)

16 L. Pan, H. J. Liu, X. J. Tan, H. Y. Lv, J. Shi, X. F. Tang, G. Zheng, Phys. Chem. Chem. Phys., 14, 13588-13593 (2012).

17 Y.-W. Son, M.L. Cohen, and S.G. Louie, Nature (London), 444, 347 (2006)

18 L.Pisani, J.A. Chan, B. Montanari,N. M. Harrison, Phys. Rev.B75, 064418 (2007)

19 H. Haugen, D.Huertas-Hernando, A. Brataas, Phys. Rev. B 77, 115406 (2008).

20 H.B.Heersche,   P.Jarillo-Herrero,   J.B.Oestinga, L.M.Vandersypen, A.F.Morpurgo, Nature 446, 56 (2007).

21 W. Y. Kim and K. S. Kim, Nature Nanotechnology 3, 408 (2008).

22 X. H. Zheng, J. Lan, X. L. Wang, L. F. Huang, H. Hao and Z. Zeng, Appl. Phys. Lett. 101, 053101 (2012).

23 J. Li, Z.H. Zhang, D. Wang, Z. Zhu, Z.Q. Fan, G.P. Tang, X.Q. Deng, Carbon 69, 142 (2014).

24 D. Wang, Z.H. Zhang, Z. Zhu, Z.L. Yu, B.K. Tao, S.Y. Hou, C. Ye, Organic Electronics 15, 3406 (2014).

25 K.Zberecki, R. Swirkowicz, J. Barnaś, Phys. Rev B (2014)

26 K.Zberecki, R. Swirkowicz, M.Wierzbicki, J. Barnaś, Phys. Chem. Chem. Phys 2014

27 L.Sun, Y.Li, Z.Li, Q.Li, Z.Zhou, Z.Chen, J.Yang, J.G.Hou, J. Chem. Phys. 129, 174114 (2008).

28 E.Bkaroglu, M.Topsakal, S.Cahangirov, S.Ciraci, Phys. Rev. B, 81, 075433 (2010).

29 L.Z.Pei,Y.H.Tang, Y.W.Chen, C.Guo, X.X.Li, Y.Yuan, Y.Zhang, J. Appl. Phys. 99, 114306 (2005).

30 Y.T.Yanga, R.X.Dinga, J.X.Songa, Phys. B, 406, 216 (2011).

31 H.Dai,E.W.Wong, Y.Z.Lu, S.Fan, C.M.Lieber, Nature 375, 769 (1995).

32 P.Pochet, L.Genovese, D.Caliste, L.Rousseau, S.Goedecker, T.Deutsch, Phys. Rev. B 82, 035431 (2010).

33 Y.Miyamoto, B.D.Yu, Appl. Phys. Lett. 80, 586 (2002).

34 X.-H.Sun, PC.P.Li, W.K.Wong, N.B.Wong, C.S.Lee, S.T.Lee, B.-K.Teo, J. Am. Chem. Soc. 124, 14464 (2002).

35 H.Zhang, W.Ding, K.He, M.Li, Nanoscale Res. Lett. 5, 1264 (2010).

36 A.Lopez-Bezanilla, J.Huang, P.R.C.Kent, B.G.Sumpter, J. Phys. Chem. C 117, 15447 (2013)

37 J.M.Zhang, F.L.Zheng, Y.Zhang, V.Ji, J. Mater Sci. 45, 3259 (2010).

38 P.Lou, Phys. Chem. Chem. Phys. 13, 17194 (2011).

39 P.Lou, J.Y.Lee, J. Phys. Chem. C 113, 21213 (2009).

40 J. Guan, W. Chen, X. Zhao, G. Yu, X. H. and Ch. Sun, J. Mater. Chem. 22, 24166 (2012).

41 J Guan, G Yu, X Ding, W Chen, Z Shi, X Huang and Ch Sun, Chem. Phys. Chem. 14, 2841 (2013).

42 P. Lou, Phys. Stat. Sol. B 250, 1265 (2013).

43 W. Chen, H. Zhang, X. Ding, G. Yu, D. Liu and X. Huang, J. Mater. Chem. C 2, 7836 (2014).

44 X. Ding, G. Yu, X. Huang and W. Chen, Phys.Chem. Chem. Phys. 15, 18039 (2013).

45 M.Wu, X.Wu, Y.Pei, X.C.Zheng, Nano Res. 4, 233 (2011).

46 P.Lou, J. Mater. Chem. C 1, 2996 (2013).

47 Y.Ding, Y.Wang, Appl. Phys. Lett. 101, 013102 (2012).

48 MOPAC2012, James J. P. Stewart, Stewart Computational Chemistry, version 14.045 web: http://openmopac.net

49 J. D. C. Maia, et al., *J. Chem. Theory Comput.* **8** (2012) 3072

50 J. J. P. Stewart, *J. Mol. Mod.* **19** (2013) 1

51 K. Parlinski, J. Phys. Conf. Series **92** (2013) 012009

52 J. Zimmermann, P. Pavone, G. Cuniberti, *Phys. .Rev.* **B 78** (2008) 045410

53 D. Sanchez-Portal, P. Ordejon, E. Artacho, J. M. Soler,Int. J. Quantum Chem. 65, 453 (1997).

54 M. Brandbyge, J.-L. Mozos, P. Ordejon, J. Taylor, K. Stokbro, Phys. Rev. B 65, 165401 (2002).

55 J.P. Perdew, K. Burke, and M. Ernzerhof. Phys. Rev. Lett., 77, 3865 (1996).

56 Ch. Lee, W. Yang and R. G. Parr, Phys. Rev. B 37 (2): 785789 (1988).